JACS
JOURNAL OF THE AMERICAN CHEMICAL SOCIETY
pubs.acs.org/JACS
Article

Multivalent Pattern Recognition through Control of Nano-Spacing in Low-Valency Super-Selective Materials

Hale Bila, Kaltrina Paloja, Vincenzo Caroprese, Artem Kononenko, and Maartje M.C. Bastings*

Cite This: J. Am. Chem. Soc. 2022, 144, 21576−21586

ABSTRACT: Super-selective multivalent ligand−receptor interactions display a signature step-like onset in binding when meeting a characteristic density of target receptors. Materials engineered for super-selective binding generally display a high number of flexible ligands to enhance the systems' avidity. In many biological processes, however, ligands are present in moderate copy numbers and arranged in spatio-temporal patterns. In this low-valency regime, the rigidity of the ligand-presenting architecture plays a critical role in the selectivity of the multivalent complex through decrease of the entropic penalty of binding. Exploiting the precision in spatial design inherent to the DNA nanotechnology, we engineered a library of rigid architectures to explore how valency, affinity, and nano-spacing control the presence of super-selectivity in multivalent binding. A micromolar monovalent affinity was required for super-selective binding to be observed within low-valency systems, and the transition point for stable interactions was measured at hexavalent ligand presentation, setting the limits of the low-valency regime. Super-selective binding was observed for all hexavalent architectures, and, more strikingly, the ligand pattern determined the selectivity onset. Hereby, we demonstrate for the first time that nano-control of geometric patterns can be used to discriminate between receptor densities in a super-selective manner. Materials that were indistinguishable in their molecular composition and ligand valency bound with various efficacies on surfaces with constant receptor densities. We define this new phenomenon in super-selective binding as multivalent pattern recognition.

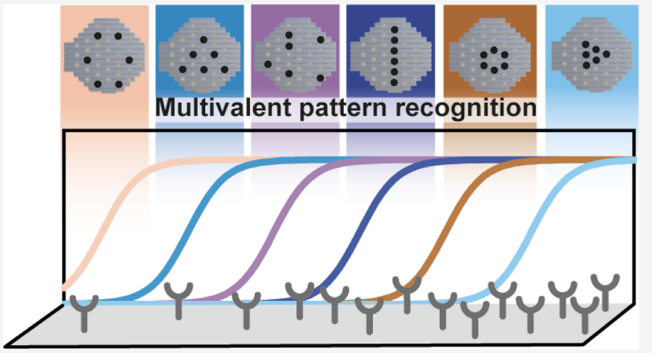

INTRODUCTION

Multivalency, strength in numbers, is an omnipresent phenomenon enhancing a ligand−receptor (L−R) interaction potential.[1,2] Natural multivalent interactions allow for cellular communication and regulation of signaling pathways,[3] whereas in chemistry, multivalency controls selectivity of bond formation and guides the supramolecular self-assembly and organization of macromolecules.[4] The classical lock-and-key analogy[5] to describe an L−R complex suggests that a single specific interaction would suffice to ensure functional binding. However, nature often chooses to employ weak monovalent couples presented in a multivalent system to ensure reversibility of the interaction as well as create an activation threshold to improve the systems' robustness.[2,6] The success of an enhanced binding strength through the presentation of multiple connected ligands mainly relies on an increased avidity toward the receptor, a boost in local concentration of ligands after a first binding event takes place.[7] The overall interaction strength and longevity are then a balance of entropic and enthalpic gains and penalties, which depend on a multitude of parameters including the flexibility of the system and the monovalent binding strength.[8,9]

Natural and synthetic multivalent interactions have been studied in great depth, and models of multivalent binding exist for both solution and surface interactions.[2,4,10,11] Through presentation of ligands in a multivalent fashion and inclusion of heterogeneous and repulsive interactions, materials with a binding behavior that ranges from a statistical enhancement due to multiple interactions to super-selective[12,13] and most recently range-selective[14] have been engineered. These specialized scenarios of multivalent L−R interactions exploit differences in receptor density and engagement of multiple weak interactions to engineer a selective onset in binding. While critical in our fundamental understanding of multivalent binding, materials that show super-selective binding[12,14−18] are built on two design strategies: (1) either the ligands are abundantly present in high valency or (2) the system is dynamic and allows for the reorganization of ligands or receptors in space to accommodate a functional interaction, which comes with an entropic penalty upon binding.[19]

Received: August 11, 2022
Published: November 16, 2022

https://doi.org/10.1021/jacs.2c08529
J. Am. Chem. Soc. 2022, 144, 21576−21586

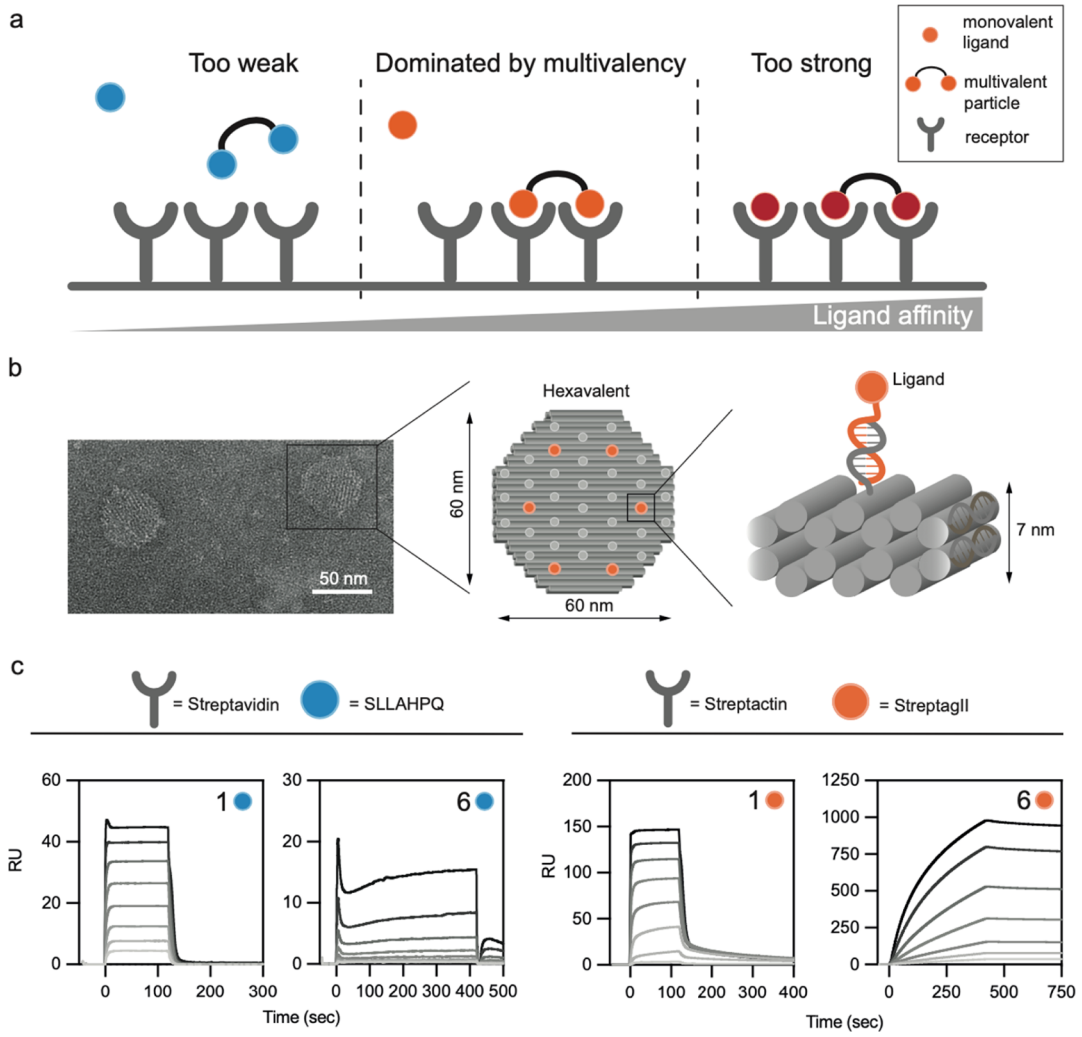

Figure 1. How weak is weak enough? (a) Schematic outline of the effect of affinity on the balance of mono *vs* multivalent interactions. The effect of multivalent binding is only significant in a limited affinity regime. (b) Negative stain transmission electron microscopy and cartoon design of the DNA-origami multivalent scaffold; each dot represents a potential ligand-presentation site that can be functionalized using complementary ssDNA attached to a ligand of choice. (c) SPR binding curves of monovalent and hexavalent binding for both L−R couples. Curves represent increasing particle concentrations, and experiments were performed in duplicate.

Within a functional interaction complex in nature, the numbers of ligands and receptors are often low-to-moderate and their position in space can be (temporally) controlled.[20] Spatial organization of ligands is typically observed in pathogens (viruses), and our immune system is highly developed to recognize such patterns.[21] In microbiology, a classical well-defined system is seen in the multivalent interaction between the bacterial phages and their target receptor used in phage display.[22] Based on spatially constrained, multivalent interactions, the best binder amongst millions of competitors can be selected, generally showcasing pM affinities. Other examples are antibodies and antigens, regarded as a significant route to initiate immunity. Recent insights in spatial tolerance of various classes of antibodies show a distinct relation between flexibility and function.[23] The multivalent IgM engages dynamically with antigen patterns on pathogens that display a wide range of spatial organization; hence, the spatial tolerance and flexibility of IgM are exceptional, ranging between 3 and 29 nm. On the contrary, the more rigid and bivalent IgG displays a lower spatial tolerance and forces a match between ligand and receptor spacing, allowing for a more stepwise, super-selective, binding profile.[23−25] On the receptor side, local density on the cell surface can be controlled through various dynamic mechanisms,[20] hence providing an avenue to enable super-selective multivalent binding. Taken together, low valency and spatially constrained architectures seem to be nature's choice when super-selective binding is assumed.

Currently, no materials exist that explore super-selective multivalent binding in the low valency regime, using a limited spatial tolerance in both the ligand and receptor presentation, as well as an exhaustible number of binding partners. We therefore wondered if super-selective multivalent binding could be engineered in low-valency materials when L−R interactions are carefully controlled in space, much similar to the examples seen in nature. Presentation of ligands in low spatial-tolerant patterns is possible when the material backbone is rigid, and the self-assembly of all components can be controlled on the molecular level. To this end, DNA nanotechnology[26−30] poses itself as the ideal engineering platform to orchestrate spatially controlled multivalent ligand presentation. The global self-assembly size, shape, and valency is directly linked to the DNA sequence and its Watson−Crick base-pairing. The structure's

https://doi.org/10.1021/jacs.2c08529
J. Am. Chem. Soc. 2022, 144, 21576−21586

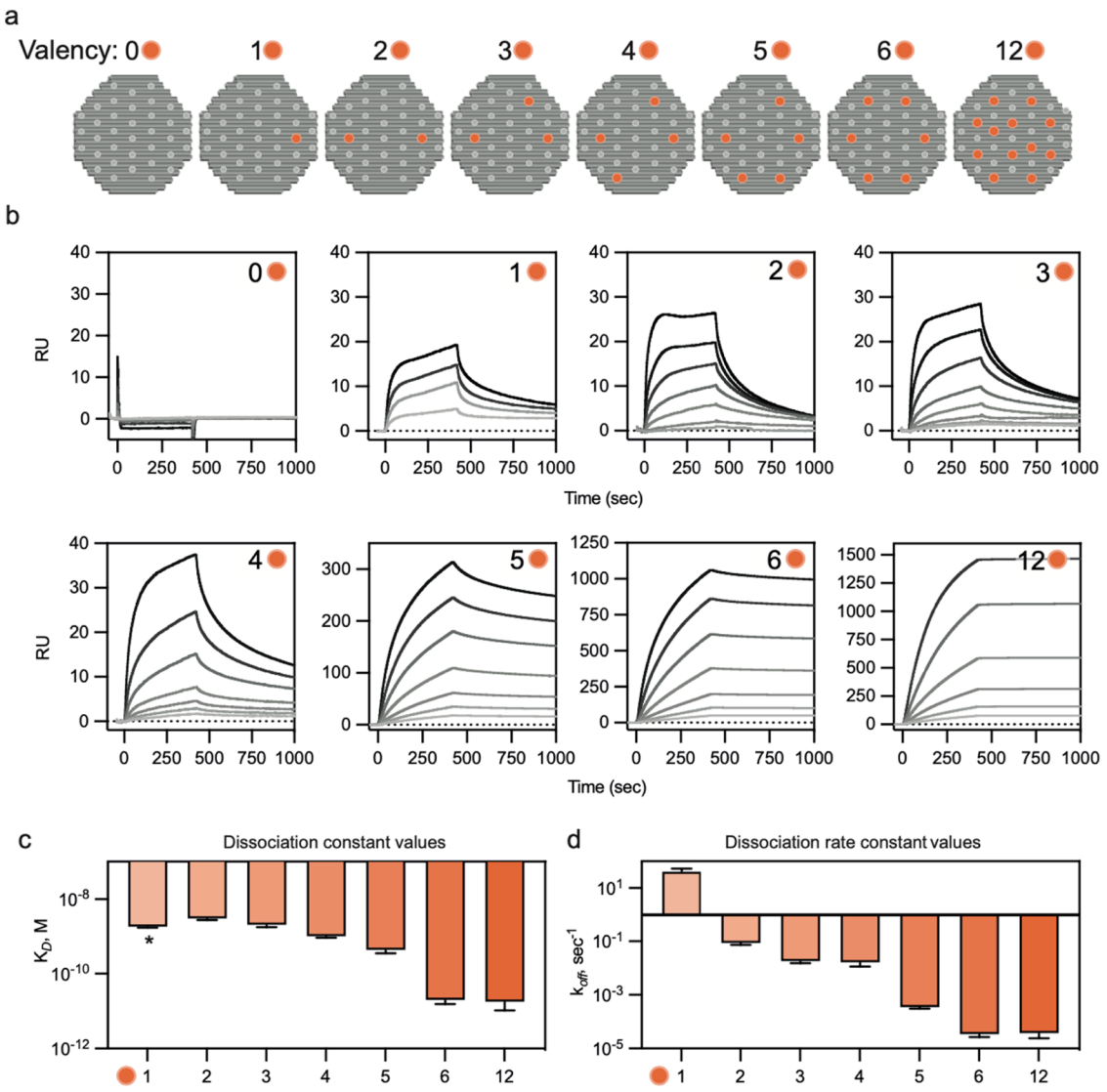

Figure 2. Analysis of the low-valency regime. (a) Schematic of the valency library from mono- to dodecavalent. (b) SPR binding curves of the valency library showing two regimes of binding: 1−4 ligands show weak interaction, while 5 and up demonstrate a strong multivalency effect. Curves represent increasing particle concentrations, and all injections were performed in duplicate. (c) Overview of dissociation constants, obtained from fitting of the SPR curves. (d) Overview of dissociation rate constants for all constructs. (*) Monovalent interaction falls outside the systems' detection limit and should be taken as an indication rather than as a quantitative value. Data presented in (c,d) as mean with error bars ± stdev from duplicate experiments.

rigidity is related to sequence length (e.g., persistence length of the DNA double helix)[31] as well as single- or double-stranded interactions.[32] Finally, the complexity of DNA-based architectures ranges from low (a single helix) to very high, in the case of DNA-origami where hundreds of strands self-assemble into a macromolecular architecture of virtually any desired shape.[28,29,33,34] Indeed, DNA-based nanomaterials have been used to explore the multivalent clustering of active cell surface receptors, and the importance of spatial organization was recently demonstrated in the case of apoptosis,[35,36] integrin targeting,[37] and focal adhesion formation.[38] The selective effect of patterns has been demonstrated in targeting of the dengue viral surface with aptamers organized in DNA star motifs.[39] Additionally, the intracellular spacing of the TLR9 immune activation receptor was found to be critically sensitive to the nano-spacing of its CpG ligand in dimeric form.[40] Both extracellular and intracellular examples show how spatially controlled low-valency interactions in nature are used to interfere with signaling pathways; however, the mechanism behind spatially controlled binding remains largely underexplored. As natural systems are subject to a plethora of complex networks, model systems can help decouple the relevant parameters that govern selective interactions. Here, we set out to study the importance of ligand affinity, controlled (low) valency, and spatial organization as deterministic parameters for super-selective binding and to further understand the fundamental biophysics behind these spatially controlled multivalent interactions.

RESULTS AND DISCUSSION

Setting the Affinity Limit: How Weak Is Strong Enough? For multivalent binding to be sensitive to valency and spatial patterns, the monovalent interaction between ligand and receptor cannot be too strong as this would forgo the need for a multivalent presentation (Figure 1a). Additionally, the difference between the monovalent and multivalent interactions should be significantly large to benefit from a multivalent ligand presentation.[16] This can be achieved with L−R couples that

https://doi.org/10.1021/jacs.2c08529
J. Am. Chem. Soc. 2022, 144, 21576−21586

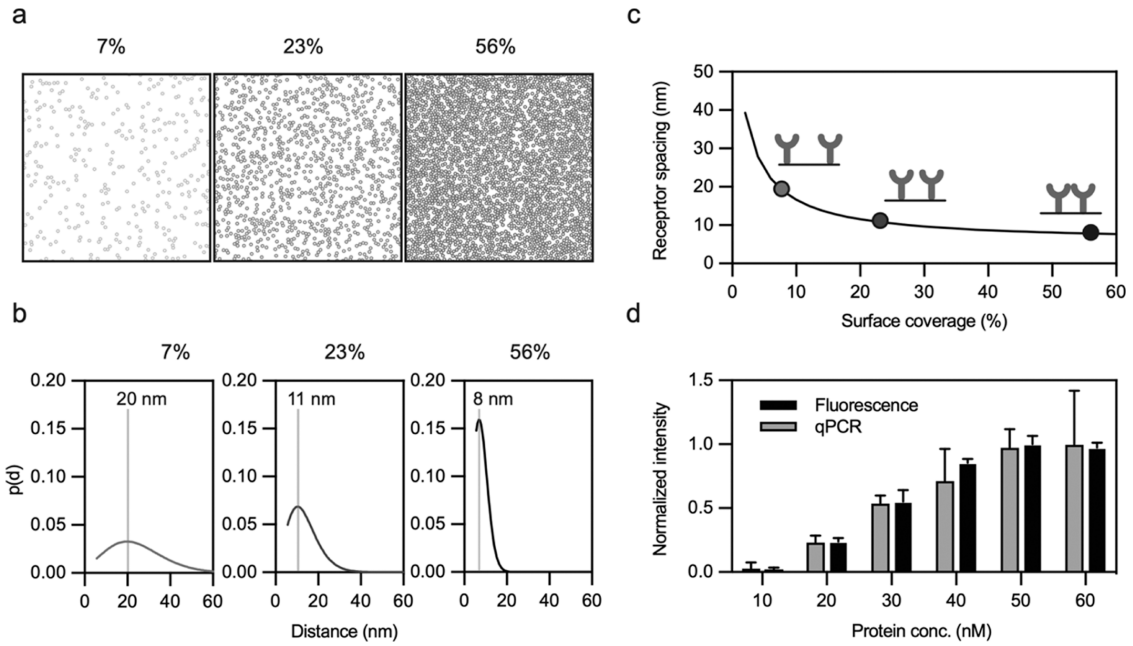

Figure 3. Calculation and preparation of surfaces with varying receptor densities. (a) Random receptor models generated by placing decreasing densities (7, 23, and 56%) of receptor particles with a random sequential adsorption distribution on a surface. (b) Probability density function $p(d)$ of the three model surfaces, showing the most abundant inter-receptor spacing per density. (c) Master curve of receptor spacing as a function of receptor density, assuming a random surface distribution. (d) Experimental characterization of test surfaces with increasing receptor spacing using both a solid phase binding assay and qPCR. Data presented as mean with error bars ± stdev from triplicate experiments.

show a moderately fast dissociation rate constant (k_{off}) as a fast dissociation favors multivalent presentation since monovalent interactions will not be stable. To prevent variations in binding behavior based on non-specific interactions or repulsion caused by the chemical or physical identity of the L−R complex, it is important to select a family of L−R couples that can span a range of affinities without significant changes in either the ligand or the receptor structure. The tetrameric protein streptavidin (SA) is well known for its extremely strong non-covalent interaction with biotin;[41] moreover, many peptide ligands have been engineered that interact with the biotin binding pocket, albeit with a lower affinity. We selected SA—SLLAHPQ (HPQ) peptide[42] and streptactin (ST)—streptagII (STII)[43] as our L−R candidates. These two systems are very similar in terms of their molecular interaction, yet theoretically show 2 orders of magnitude difference in the monovalent dissociation constant, K_D: ∼100 μM for SA-HPQ[42] and ∼1 μM for ST−STII.[44] The additional advantage of using a multimeric protein (SA or ST) for surface binding studies is that regardless of the orientation of surface immobilization, at least one binding pocket will always be available. Both HPQ and STII peptides were synthesized on the solid phase and site-specifically coupled using thiol-maleimide chemistry to a single strand (ss) DNA on their C-terminus (Figure S1).

Spacing of ligands as the controlling parameter of super-selective binding is only relevant if the scaffold is rigid on the nanoscale, uniform, and precisely defined in space. We previously reported on the synthesis of a DNA-origami disk, presenting 36 periodically spaced functionalization "pixels" on each face.[45] This particle allows for a modular display of ligands in a large range of valencies, spacings, and patterns. Additionally, relying on the robustness of DNA sequence-specific hybridization, all particles can be assumed to be identical with very high confidence. Hexavalent architectures were generated by annealing of the ssDNA-peptide ligands with a DNA-disk scaffold (Figure 1b), which presented the complementary ssDNA handles in predetermined positions, and purity was confirmed by gel electrophoresis (Figure S2). Surface plasmon resonance (SPR) analysis was then performed to obtain the affinity and kinetic binding parameters (Figure 1c). Nonspecific interactions were excluded as non-functionalized (bare) scaffolds and scrambled peptides did not show any binding to the test surface (Figure S3). The monovalent affinity constants were found to be ∼60 and ∼3 μM for HPQ and STII, respectively, matching literature values. Interestingly, while the overall affinity was improved, the hexavalent presentation of the HPQ peptide did not yield a stable interaction due to fast off-rates, making the system too weak to be operational in the low valency regime. On the contrary, when STII was presented in a hexavalent pattern, a strong multivalency effect was observed, gaining 3 orders in affinity and off-rates slowed down by 5 orders of magnitude. These results demonstrate that not only the overall K_D is of importance in the design of super-selective materials, but it is equally important to consider the kinetic parameters of binding.[46,47] For all next experiments, the ST−STII couple was employed.

Exploring the Low-Valency Regime: How Few Is Enough? As multivalency is "strength in numbers", it might be tempting to take an "as many as possible" approach when it comes to ligand functionalization on the nanomaterial surface. Indeed, the presence of more ligands increases the statistical probability of binding and thereby affects the systems' avidity.[7] Present literature examples where strong super-selective interactions have been measured used high ligand valencies. However, when interactions on a surface are concerned, many ligands in these high-valency systems will not actively participate in binding, yielding a redundancy in design. While not always problematic, these non-bound ligands could cause significant issues when involved in cellular signaling processes or trigger an uncontrolled immune response. Based on the theory of super-

https://doi.org/10.1021/jacs.2c08529
J. Am. Chem. Soc. 2022, 144, 21576−21586

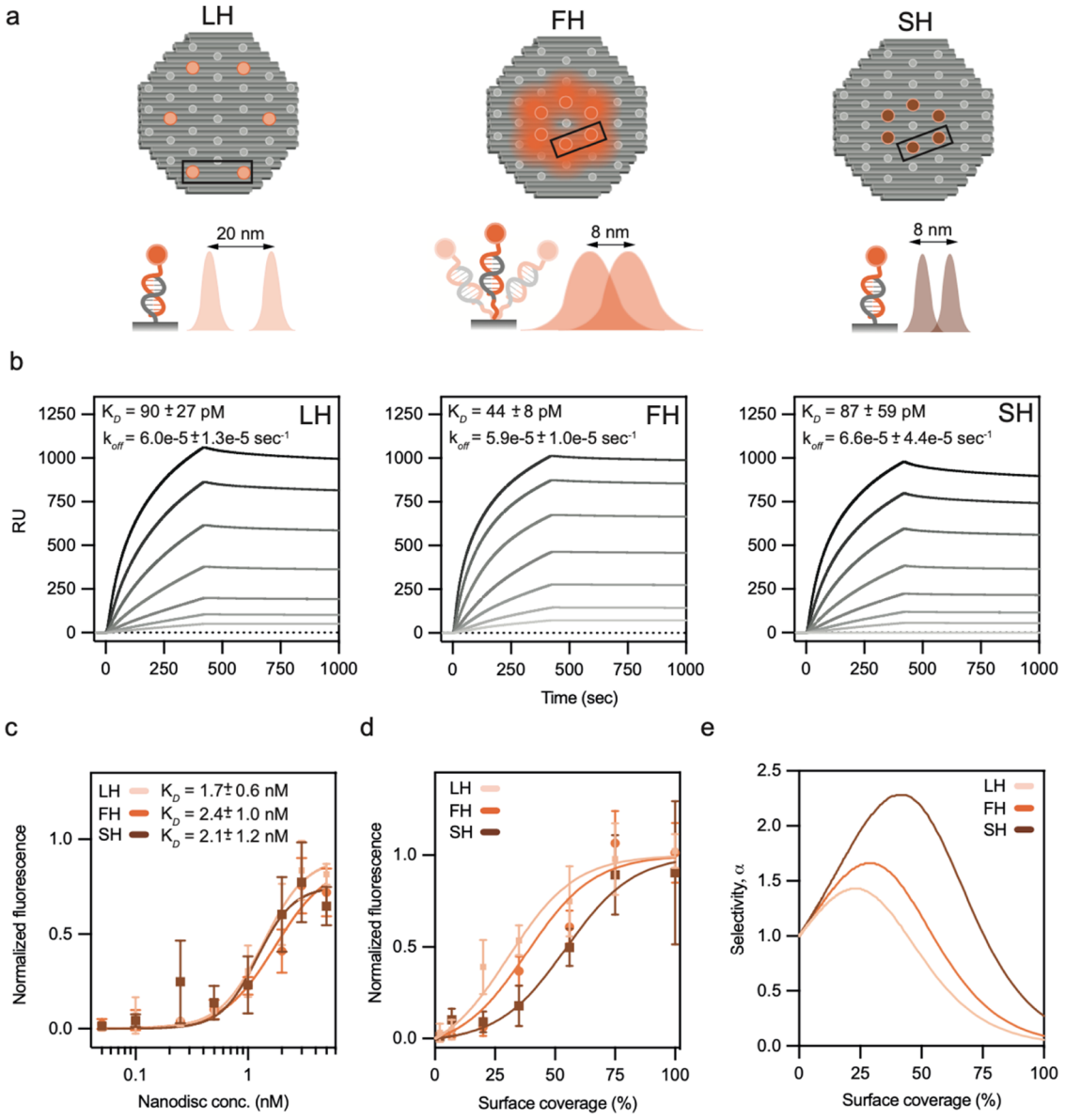

Figure 4. Super-selective binding with hexagonal rigid and flexible patterns. (a) Ligand spacing and spatial tolerance of hexagonal patterns. (b) SPR binding curves of LH, SH, and FH confirming identical affinities. Curves represent increasing particle concentrations and all injections were performed in duplicate. (c) Solid-phase binding assay of LH, SH, and FH at 100% receptor density. Data presented as mean with error bars ± stdev from n = 5 in duplicate experiments. (d) Density-dependent onset of multivalent binding at a fixed ligand concentration. Data presented as mean with error bars ± stdev from n = 20 in duplicate experiments. (e) Super-selectivity parameter α for hexagonal arrays.

selectivity, the theoretical gain in selectivity of binding after pentavalent ligand presentation is minimal. We therefore decided to experimentally test the effect of valency and analyze how "low" is "high enough" to benefit from the multivalency effect and define the "low-valency regime" within the context of potential super-selective interactions.

In earlier work, the high spatial confidence of functional nanopatterns on DNA-origami disks was demonstrated.[45] Using this DNA disk, we generated a particle library of increasing ligand valency, 1-2-3-4-5-6-12 (Figures 2a, S4) and measured their binding profiles with SPR (Figure 2b). The non-liganded disk was used to exclude non-specific interactions and indeed shows no binding to the target receptor. Up to tetravalent ligand presentation, a relatively fast dissociation was observed, which started to slow down at pentavalent ligand valency. The monovalent interaction is so weak that no reliable SPR data could be obtained using the 60 nM concentration limit given by DNA-origami nanomaterials. Interestingly, a strong and stable multivalent binding was seen when five or more ligands were presented, as reflected in the K_D shifting to low pM concentrations and k_{off} under ~10^{-5} sec^{-1} (Figure 2c,d). Affinity and kinetics slightly improved for hexavalent arrays, but, in line with the theoretical models,[13] additional increase to dodecavalent did not further enhance the interaction significantly. We conclude that a hexavalent interaction presents the limit of the low-valency regime.

Engineering of Receptor Density-Controlled Model Surfaces. Control over the receptor density on assay surfaces is critical to characterize super-selectivity. The density of receptors on a surface is inversely related to the distance between them: the higher the density, the smaller the inter-receptor distance. In an ideal case, the "perfect" density-controlled surface would be

https://doi.org/10.1021/jacs.2c08529
J. Am. Chem. Soc. 2022, 144, 21576−21586

one where all receptors are placed on a lattice with integer spacing. More realistically, resembling proteins on a cell membrane, receptors are randomly distributed, and their distribution fluctuates around an average spacing value.[20,48−50] Within rigid materials, the spacing (y) between ligands is fixed; hence, it is important to quantify the average receptor spacing (x) of first neighbors on a test surface, as when $x > y$, strong multivalent binding is compromised. Naturally, starting at $x = y$, a density-dependent onset of binding—characteristic for super-selective interactions—can be anticipated.

To model the average distribution of receptors on a surface, we randomly positioned decreasing numbers of receptors following a random sequential adsorption model (Figure 3a) and calculated the inter-receptor probability distributions (Figures 3b, S5). For sufficiently dense surfaces, a characteristic receptor spacing can be seen. Of note is that on sparce surfaces, the $p(d)$ increasingly widens, for example, a distinctive distance is not present. Via simulation of the receptor distribution on a surface at a given density (methods in the Supporting Information), we obtained a master curve of the inter-receptor spacing (Figure 3c). Solid phase and quantitative (q-)PCR analysis were used to empirically obtain the conditions needed to reach the plateau of protein density, corresponding to a 100% surface density (Figure S6). A density series of ST surfaces ranging from 2 to 100% (e.g., receptor spacings of 38 and 7 nm, respectively) was obtained using decreasing concentrations of ST in the immobilization protocol[42] and confirmed with qPCR and solid phase binding (Figure 3d). Any remaining surface area was blocked with BSA in order to prevent nonspecific binding. Matching the spacing (x) of receptors to the end-to-end distance (y) of any hexavalent ligand array, we can now derive the experimental preparation guidelines and suggested regimes by which to expect onset of potential super-selective binding.

Super-Selective Binding and the Effect of Spatial Tolerance in Hexavalent Systems. As the initial hexavalent array, we decided to focus on a hexagonal ligand pattern as this is a symmetric geometry often found in nature.[51] Since we were curious about the effect of nano-rigidity on the onset of super-selective binding, we generated variations of the hexagonal ligand arrays, capitalizing on the variations in mechanical properties of double- *versus* single-stranded DNA.[52] The spacing of the ligands in the hexagonal array was controlled through selection of different functional sites on the DNA-origami disk, resulting in a large hexagon (LH) and small hexagon (SH) patterns (Figure 4a). The rigidity of the SH was modified via the inclusion of 5 nt single-stranded sections in the functional handles on the disk (flexible hexagon, FH). Of note is that the adjective "flexible" signifies the enlarged spatial tolerance of the peptide ligand as the full DNA-origami structure is still highly rigid and all ligands are pre-oriented to the plane of interaction in order to reduce conformational entropic penalties of binding. Distances of functionalization points of LH and SH patterned DNA-origami disks were measured previously by DNA-PAINT and found to be ∼20 nm for LH and ∼8 for SH;[45] the flexible extensions introduce an estimated spatial flexibility of ∼4 nm (Figure S7). Applying the master curve of receptor spacing (Figure 3c), we can extract the ideal receptor density for each hexagonal array: the LH corresponds to 7% (= 20 nm), and SH matches with 56% (= 8 nm). The FH pattern is expected to interact with a range of densities, starting at 23% (= 11 nm).

In the absence of any repulsive force, the strongest affinity of a multivalent particle is measured at the highest receptor density as the Langmuir isotherm of the occupied surface is at its maximum.[13] Since the analytical method used can influence or bias the affinity parameters,[42] SPR as well as a solid-phase surface assay were combined to obtain both static (Figure 4b) and kinetic affinity data (Figure 4c). The slight underestimation of affinity using solid-phase analysis results from the detection limit in the low pM particle concentrations. Within both techniques, no differences between the three hexagonal ligand arrays were detected. This was expected since the rigid DNA backbone pre-orients ligands to the same plane to favor binding; hence, the conformational entropic penalty is minimal. The added flexibility in FH is therefore only significant for the ligand spacing, for example, overall spatial tolerance of the system. Any potential difference in super-selective behavior between the hexagonal constructs is thus a result of ligand pattern or spatial tolerance and not caused by a favorable overall affinity.

Next, we aimed to explore if super-selective binding behavior was present in these low-valency particles, and to what extent spatial tolerance is critical. The affinity data of the lower valency arrays provided the concentration range for the super-selectivity experiments as these should be performed above the K_D but below the concentration where an onset of lower valency can blur the pattern recognition effect. The working concentration for all hexavalent particles was set as 3 nM, which is an order of magnitude lower than the bi- and trivalent constructs, thereby preventing any interference of lower valency interactions. While matching the K_D of tetra- and pentavalent constructs, the differences in dissociation rate constant favor the hexavalent interaction as the dominant readout. We prepared test surfaces matching the pattern spacing of the three hexavalent disks (7, 23, and 56% for LH, FH, and SH respectively) as well as higher and lower values to evaluate a wide range of receptor densities. Solid-phase binding assays convincingly showed the super-selective multivalent binding in the low-valency regime (Figure 4d) as a steep switch-like response was observed for all particles. Furthermore, all particles showed an onset of binding in their expected respective surface densities: the rigid LH starts binding after 7% receptor density, followed by FH at 23%. Only SH is interacting earlier than the expected 56%; however, as can be seen in the master curve of spacing, after 30%, the inter-receptor spacing is approaching the jamming-limit asymptote. These data show the direct effect of linker-flexibility (e.g., spatial tolerance) on binding onset as FH is based on the SH pattern, but with a larger distribution of the inter-ligand distance resulting from the flexible linkers. Indeed, this structure shows a higher spatial tolerance than the rigid small hexagon and as a result starts to bind at lower density surfaces. To quantify the level of super-selectivity, Frenkel et al. introduced the selectivity parameter α as a measure of the sensitivity of the binding of multivalent particles to the surface concentration of receptors.[13] α is the slope of the adsorption profile in a log−log plot and is lower than 1 for monovalent binding, while for super-selective multivalent interactions, the selectivity can reach values much greater than 1. All hexagonal binding patterns were fit and showed a super-selective interaction as the selectivity parameter α lays above 1 for all arrays (Figure 4e). The peak in selectivity strongly correlates to the regime where spacing of ligands matches spacing of receptors. For the more spatially tolerant FH, a lower selectivity was observed in line with the hypothesis that more flexibility leads to a less-defined spacing and thus lower selectivity.

MPR through Spatial Control of Ligand Geometry. Thus far, our data show that when the monovalent and multivalent affinity between a ligand−receptor couple is

https://doi.org/10.1021/jacs.2c08529
J. Am. Chem. Soc. 2022, 144, 21576−21586

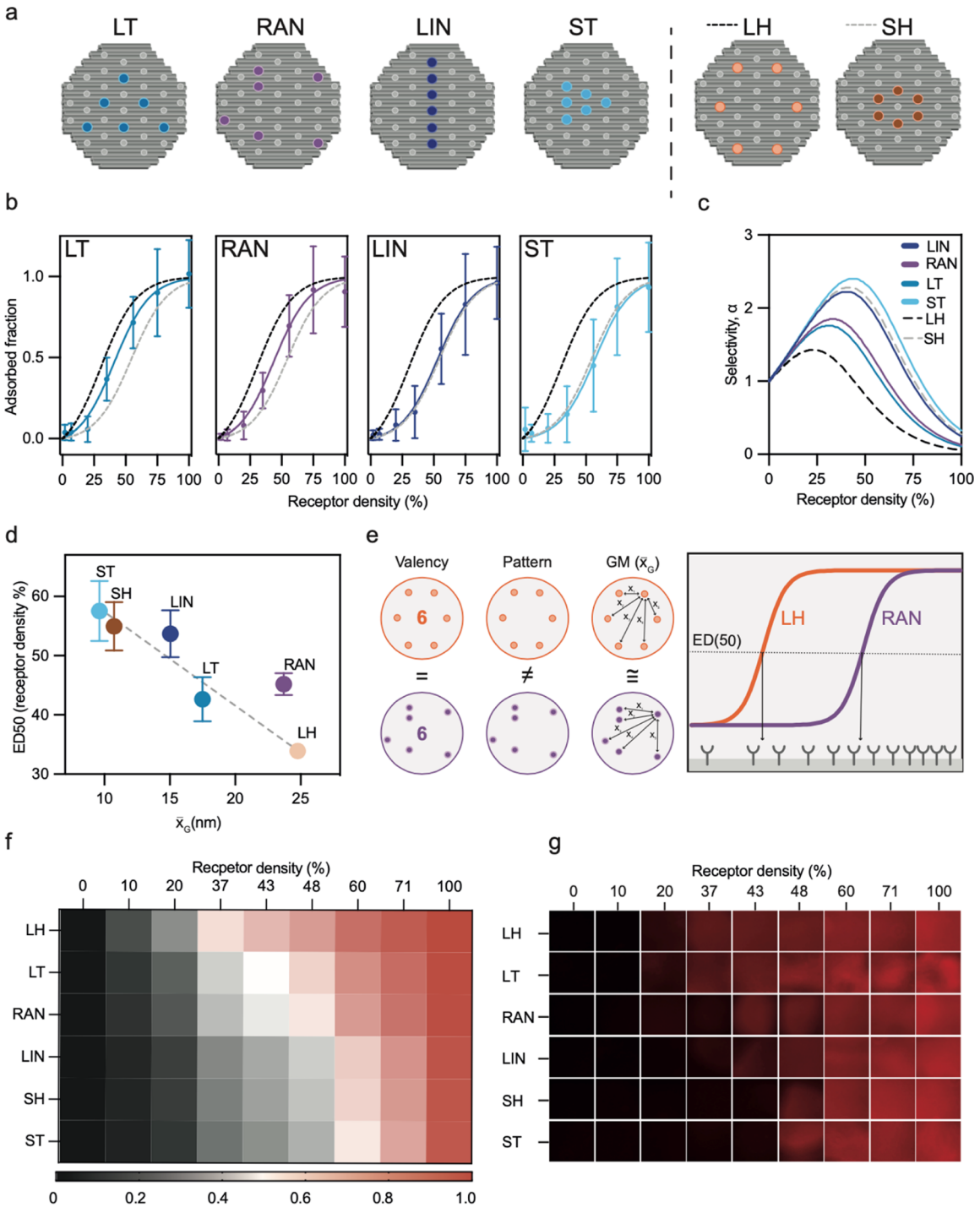

Figure 5. MPR. (a) Pattern library of hexavalent DNA disks with varying geometry: large triangle (LT), random (RAN), linear (LIN), and small triangle (ST). Large hexagon (LH) and small hexagon (SH) are included for reference. (b) Solid-phase binding assay on increasingly dense receptor surfaces (LH and SH are included for comparison in gray dotted lines). Data presented as mean with error bars ± stdev from $n = 20$ in duplicate experiments. (c) Super-selectivity parameter α for all hexavalent pattern arrays (LH and SH are included for comparison in gray dotted lines). (d) ED_{50} *vs* GM for pattern library showing the correlation of pattern to selectivity (the dotted line is the linear regression fit through patterns). (e) Highlighting the decisive role of the pattern between super-selective binding of LH and RAN. (f) Heatmap of MPR based on super-selectivity curves; color scale highlights 50% interaction. (g) Functional demonstration of MPR through imaging of various densities of receptor surfaces targeted by the hexavalent particle library.

sufficiently distinct, spatially constrained presentation of ligands can lead to super-selective binding behavior in the low-valency regime. Furthermore, the specific spatial organization and tolerance of ligands with the same valency was shown to control the selectivity. Hereby, a nuance in super-selective binding is observed that is linked to the ligand pattern and its spatial tolerance. To further explore this super-selective multivalent pattern recognition (MPR), we decided to test the binding behavior of additional variations of hexavalent ligand patterns. To this end, a linear (L), small triangle (ST), and large triangle

https://doi.org/10.1021/jacs.2c08529
J. Am. Chem. Soc. 2022, 144, 21576−21586

(LT) pattern as well as a random (RAN) setting were designed, benefitting from the modular functionalization of the pixels on the DNA disk (Figures 5a, S8). First, the affinity on 100% receptor density and kinetic binding parameters were measured and confirmed to be identical to the previous hexagonal patterns as well as within the new pattern library (Figures S9 and S10). Multivalent binding analysis on various receptor densities again showed the characteristic super-selective behavior for all patterns (Figure 5b), and the super-selectivity parameter α was found to be above 1 in all arrays (Figure 5c). Comparing all patterns, LH showed the earliest onset in binding, coherent to its largest spacing between ligands. LIN, ST, and SH show the smallest spacings between ligands and behave indeed alike in terms of onset of binding and selectivity. A similar onset of binding and selectivity for LT and RAN was observed, while their average spatial distribution between ligands is quite different. This points toward the critical effect of geometric pattern.

Looking more closely into the mathematical differences between each geometry, we decided to calculate the geometric mean (GM, $\bar{x}$) between ligands as the metric to describe each pattern. While not taking into account the angular relation between ligands, this simple approach provides a guide where binding is expected to commence. The importance of pattern over valency and average spacing becomes apparent when the 50% effective density (ED_{50}) based on the super-selectivity experiments is presented against the GM per particle (Figure 5d). For symmetric patterns, the GM can be used as a simple guide to design a tailored ligand pattern to a desired target surface. While ligand spacing provides an indicative measure for onset of binding for symmetric geometries, the contribution of the specific pattern is evident in the case of RAN *versus* LH. These particles have the same valency and a very similar geometric mean, yet the distinction in pattern contributes to the significant change in super-selective onset of binding (Figure 5e). Matching the experimental values and mathematical characterization confirms MPR is defined by geometry; additionally, we show that a pattern and its super-selective behavior can be rationally designed to any desired target receptor density.

The super-selective multivalent targeting of surfaces with low-valency materials, as demonstrated in this study, provides a new opportunity in the engineering of nanomaterials for molecular biology and diagnostics. In these fields, the nuanced and tailored control over the material−cell interface is critical, and the design of particles with predictable interactions allows us to unravel the details of signaling pathways as well as cell-specific binding. Understanding the pattern design rules to predict the "best pattern for the job" is critical to translate the concept of MPR toward a broad range of applications. We showed that the boundaries for onset of binding and level of selectivity are defined by the ligand pattern spacing, geometry, and spatial tolerance. Based on the super-selectivity curves, a heatmap of binding was generated per pattern and surface density (Figure 5f). To visually demonstrate the power of MPR, we performed a microscopy study where the library of geometric hexavalent particles was presented to various receptor surface densities. Solely through recognition of the pattern, selective multivalent binding controls the onset of interaction with the matching surface densities (Figure 5g). The obtained image of fluorescent surfaces matches excellently with the super-selectivity heatmap extracted from super-selectivity analysis (Figure 5f), showcasing the practical applicability of MPR.

CONCLUSIONS

Super-selective multivalent binding is characterized by a strong density-dependent onset of ligand−receptor complexation. Previous studies on this mechanism have explored the engineering parameters that promote the strongest super-selective behavior, being dominated by high valency and flexible ligand presentation. In the high valency regime, any influence of spatial tolerance or pattern is irrelevant as the overall avidity is dominated by the enthalpy of the many interactions formed. In this study, we focused on the low-valency regime as many signaling pathways in nature present a limited number of binding sites and use a well-defined geometry. When the ligand geometry is rigid, individual bonds either fit or they do not, which is directly correlated to the spacing of receptors. Indeed, we measured a strong receptor density effect on the onset of binding when ligand presentation was spatially constrained. Furthermore, within the low-valency regime, we showed that off rates are critical in setting a working affinity/valency balance. A monovalent affinity in the low micromolar range allowed us to visualize the power of multivalent ligand presentation, and a valency threshold of 5 was found to be the tipping point of strength in numbers in the low-valency regime. Interestingly, the pentavalent presentation of ligands often occurs in nature, for example, in toxins, phages, and capsid proteins on viruses. Addition of one more ligand into a hexavalent array slightly improved the affinity and kinetics of binding, yet the increase of ligands beyond hexavalency was shown to be irrelevant.

Besides the demonstration of super-selectivity in the low-valency regime, our data present a further nuance of super-selectivity, where the spatial organization (e.g., pattern) of ligands is the main determinant of onset of binding. Benefitting from the programmable nature of DNA nanotechnology, all six hexavalent particles have exactly the same mass, charge, size, and molecular composition. Their unique difference is the nano-spacing of the ligands. Through the use of a rigid, planar particle, all six ligands are pre-oriented toward the assay surface, thereby strongly reducing the rotational and translational entropy penalties. Hereby, the differences in interaction can be assigned directly to the spatial patterns of the ligands and their correlation to the receptor distribution. Hence, we define this nuanced form of super-selective binding as MPR. When a system's threshold pattern density is reached, a characteristic super-selective switch-like onset of binding is apparent. We observed that for the same pattern, a higher rigidity results in a stronger super-selective response (higher α value) due to a more significant reduction in the entropic penalty of conformational change. On the contrary, a higher spatial tolerance resulted in an earlier onset of binding and a lower selectivity parameter. In short, more flexible means less selective. Of note is that while the ligand patterns are fully controlled, the receptors are randomly distributed. This critical detail confirms that MPR can happen on natural surfaces where membrane receptors display a random organization, both outside and inside separate domains of higher local densities.

The significance of spatial tolerance in MPR is visible in the low-valency regime when the difference in K_D between mono- and multivalent ligand presentation is sufficiently large. When too few or too many ligands are present, binding is either too weak or the overall avidity too strong to observe the MPR effect. Nature seems to be able to intelligently play with this concept, as seen, for example, in antibody arrays that can switch between 1, 2, and 5 (or 6) for IgG, IgA, and IgM, respectively.[53,54]

https://doi.org/10.1021/jacs.2c08529
J. Am. Chem. Soc. 2022, 144, 21576−21586

Significant changes in local densities of receptors are known to occur as part of disease processes,[55] apoptosis,[35,36] and signaling in, for instance, the immune synapse.[56,57] Local high concentrations can temporarily be locked in place through changes in surrounding lipid dynamics.[20,49,58] From the receptor side, the boundary conditions for MPR and more general super-selective multivalent interactions can be easily reached. As many natural ligands are present on precisely organized scaffolds, as in the case of viruses and geometric toxin complexes,[2,59] MPR is likely to be omnipresent in molecular biology. When entering the MPR regime, materials with unique physical behavior can be designed, and we provided the mathematical guidelines to match and predict a pattern to a desired target surface. Our insights, therefore, will open novel strategies for precision medicine and super-selective diagnostics, following materials engineering advances and analysis of the rigid, low-valency nanomaterial-biointerface.

■ ASSOCIATED CONTENT

Supporting Information

The Supporting Information is available free of charge at https://pubs.acs.org/doi/10.1021/jacs.2c08529.

Materials and methods; full characterization details of ligands, particles, and surfaces; controls for non-specific binding; all SPR data; ssDNA staple sequences; and fitted parameters for the super-selectivity model and mathematical description of patterns (PDF)

■ AUTHOR INFORMATION

Corresponding Author

Maartje M.C. Bastings − *Programmable Biomaterials Laboratory (PBL), Institute of Materials (IMX), Interfaculty Bioengineering Institute (IBI), School of Engineering (STI), Ecole Polytechnique Fédérale Lausanne (EPFL), Lausanne 1015, Switzerland;* orcid.org/0000-0002-7603-4018; Email: maartje.bastings@epfl.ch

Authors

Hale Bila − *Programmable Biomaterials Laboratory (PBL), Institute of Materials (IMX), Interfaculty Bioengineering Institute (IBI), School of Engineering (STI), Ecole Polytechnique Fédérale Lausanne (EPFL), Lausanne 1015, Switzerland*

Kaltrina Paloja − *Programmable Biomaterials Laboratory (PBL), Institute of Materials (IMX), Interfaculty Bioengineering Institute (IBI), School of Engineering (STI), Ecole Polytechnique Fédérale Lausanne (EPFL), Lausanne 1015, Switzerland;* orcid.org/0000-0001-8504-9919

Vincenzo Caroprese − *Programmable Biomaterials Laboratory (PBL), Institute of Materials (IMX), Interfaculty Bioengineering Institute (IBI), School of Engineering (STI), Ecole Polytechnique Fédérale Lausanne (EPFL), Lausanne 1015, Switzerland*

Artem Kononenko − *Programmable Biomaterials Laboratory (PBL), Institute of Materials (IMX), Interfaculty Bioengineering Institute (IBI), School of Engineering (STI), Ecole Polytechnique Fédérale Lausanne (EPFL), Lausanne 1015, Switzerland;* orcid.org/0000-0001-8966-0512

Complete contact information is available at: https://pubs.acs.org/10.1021/jacs.2c08529

Author Contributions

H.B., K.P., V.C., and A.K. contributed equally to this work and all authors approved the final text and Supporting Information.

Notes

The authors declare no competing financial interest.

■ ACKNOWLEDGMENTS

This study was funded by the Swiss National Science Foundation (SNSF) by Eccellenza grant PCEGP2_181137 to M.M.C.B. The authors would like to thank Giacomo Chizzola for contributions in the early stages of the project, Dr. Marianna M. Koga for contributions in protocol development, Hugo J. Rodríguez-Franco for transmission electron microscopy imaging, and Dr. Diana Morzy for critical comments on the manuscript.

■ REFERENCES

(1) Kiessling, L. L.; Gestwicki, J. E.; Strong, L. E. Synthetic Multivalent Ligands in the Exploration of Cell-Surface Interactions. *Curr. Opin. Chem. Biol.* **2000**, *4*, 696−703.

(2) Mammen, M.; Choi, S. K.; Whitesides, G. M. Polyvalent Interactions in Biological Systems: Implications for Design and Use of Multivalent Ligands and Inhibitors. *Angew. Chem., Int. Ed. Engl.* **1998**, *37*, 2754−2794.

(3) Kiessling, L. L.; Gestwicki, J. E.; Strong, L. E. Synthetic Multivalent Ligands as Probes of Signal Transduction. *Angew. Chem., Int. Ed.* **2006**, *45*, 2348−2368.

(4) Fasting, C.; Schalley, C. A.; Weber, M.; Seitz, O.; Hecht, S.; Koksch, B.; Dernedde, J.; Graf, C.; Knapp, E.-W.; Haag, R. Multivalency as a Chemical Organization and Action Principle. *Angew. Chem., Int. Ed.* **2012**, *51*, 10472−10498.

(5) Fischer, E. The Influence of Configuration on Enzyme Activity. *Dtsch. Chem. Ges.* **1894**, *27*, 2984−2993.

(6) Lan, J.; Ge, J.; Yu, J.; Shan, S.; Zhou, H.; Fan, S.; Zhang, Q.; Shi, X.; Wang, Q.; Zhang, L.; Wang, X. Structure of the SARS-CoV-2 Spike Receptor-Binding Domain Bound to the ACE2 Receptor. *Nature* **2020**, *581*, 215−220.

(7) Erlendsson, S.; Teilum, K. Binding Revisited-Avidity in Cellular Function and Signaling. *Front. Mol. Biosci.* **2021**, *7*, 615565.

(8) Kitov, P. I.; Bundle, D. R. On the Nature of the Multivalency Effect: A Thermodynamic Model. *J. Am. Chem. Soc.* **2003**, *125*, 16271−16284.

(9) Abstiens, K.; Gregoritza, M.; Goepferich, A. M. Ligand Density and Linker Length are Critical Factors for Multivalent Nanoparticle-Receptor Interactions. *ACS Appl. Mater. Interfaces* **2019**, *11*, 1311−1320.

(10) Huskens, J. Multivalent Interactions at Interfaces. *Curr. Opin. Chem. Biol.* **2006**, *10*, 537−543.

(11) Huskens, J.; Mulder, A.; Auletta, T.; Nijhuis, C. A.; Ludden, M. J. W.; Reinhoudt, D. N. A Model for Describing the Thermodynamics of Multivalent Host−Guest Interactions at Interfaces. *J. Am. Chem. Soc.* **2004**, *126*, 6784−6797.

(12) Tian, X.; Angioletti-Uberti, S.; Battaglia, G. On the Design of Precision Nanomedicines. *Sci. Adv.* **2020**, *6*, No. eaat0919.

(13) Martinez-Veracoechea, F. J.; Frenkel, D. Designing Super Selectivity in Multivalent Nano-Particle Binding. *Proc. Natl. Acad. Sci. U.S.A.* **2011**, *108*, 10963−10968.

(14) Liu, M.; Apriceno, A.; Sipin, M.; Scarpa, E.; Rodriguez-Arco, L.; Poma, A.; Marchello, G.; Battaglia, G.; Angioletti-Uberti, S. Combinatorial Entropy Behaviour Leads to Range Selective Binding in Ligand-Receptor Interactions. *Nat. Commun.* **2020**, *11*, 4836.

(15) Wang, J.; Min, J.; Eghtesadi, S. A.; Kane, R. S.; Chilkoti, A. Quantitative Study of the Interaction of Multivalent Ligand-Modified Nanoparticles with Breast Cancer Cells with Tunable Receptor Density. *ACS Nano* **2020**, *14*, 372−383.

(16) Scheepers, M. R. W.; van IJzendoorn, L. J.; Prins, M. W. J. Multivalent Weak Interactions Enhance Selectivity of Interparticle Binding. *Proc. Natl. Acad. Sci. U.S.A.* **2020**, *117*, 22690−22697.
(17) Linne, C.; Visco, D.; Angioletti-Uberti, S.; Laan, L.; Kraft, D. J. Direct Visualization of Superselective Colloid-Surface Binding Mediated by Multivalent Interactions. *Proc. Natl. Acad. Sci. U.S.A.* **2021**, *118*, No. e2106036118.
(18) Dubacheva, G. V.; Curk, T.; Mognetti, B. M.; Auzély-Velty, R.; Frenkel, D.; Richter, R. P. Superselective Targeting Using Multivalent Polymers. *J. Am. Chem. Soc.* **2014**, *136*, 1722−1725.
(19) Martinez-Veracoechea, F. J.; Leunissen, M. E. The Entropic Impact of Tethering, Multivalency and Dynamic Recruitment in Systems with Specific Binding Groups. *Soft Matter* **2013**, *9*, 3213.
(20) Morzy, D.; Bastings, M. Significance of Receptor Mobility in Multivalent Binding on Lipid Membranes. *Angew. Chem., Int. Ed.* **2022**, *61*, No. e202114167.
(21) Kawai, T.; Akira, S. The Role of Pattern-Recognition Receptors in Innate Immunity: Update on Toll-like Receptors. *Nat. Immunol.* **2010**, *11*, 373−384.
(22) Smith, G. P.; Petrenko, V. A. Phage Display. *Chem. Rev.* **1997**, *97*, 391−410.
(23) Shaw, A.; Hoffecker, I. T.; Smyrlaki, I.; Rosa, J.; Grevys, A.; Bratlie, D.; Sandlie, I.; Michaelsen, T. E.; Andersen, J. T.; Högberg, B. Binding to Nanopatterned Antigens Is Dominated by the Spatial Tolerance of Antibodies. *Nat. Nanotechnol.* **2019**, *14*, 184−190.
(24) Jendroszek, A.; Kjaergaard, M. Nanoscale Spatial Dependence of Avidity in an IgG1 Antibody. *Sci. Rep.* **2021**, *11*, 12663.
(25) Zhang, P.; Liu, X.; Liu, P.; Wang, F.; Ariyama, H.; Ando, T.; Lin, J.; Wang, L.; Hu, J.; Li, B.; Fan, C. Capturing Transient Antibody Conformations with DNA Origami Epitopes. *Nat. Commun.* **2020**, *11*, 3114.
(26) Seeman, N. C.; Sleiman, H. F. DNA Nanotechnology. *Nat. Rev. Mater.* **2017**, *3*, 17068.
(27) Linko, V.; Dietz, H. The Enabled State of DNA Nanotechnology. *Curr. Opin. Biotechnol.* **2013**, *24*, 555−561.
(28) Douglas, S. M.; Dietz, H.; Liedl, T.; Högberg, F.; Graf, W. M.; Shih, B. Self-Assembly of DNA into Nanoscale Three-Dimensional Shapes. *Nature* **2009**, *459*, 414−418.
(29) Rothemund, P. W. K. Folding DNA to Create Nanoscale Shapes and Patterns. *Nature* **2006**, *440*, 297−302.
(30) Seeman, N. C. Nanomaterials Based on DNA. *Annu. Rev. Biochem.* **2010**, *79*, 65−87.
(31) Manning, G. S. The Persistence Length of DNA Is Reached from the Persistence Length of Its Null Isomer through an Internal Electrostatic Stretching Force. *Biophys. J.* **2006**, *91*, 3607−3616.
(32) Murphy, M. C.; Rasnik, I.; Cheng, W.; Lohman, T. M.; Ha, T. Probing Single-Stranded DNA Conformational Flexibility Using Fluorescence Spectroscopy. *Biophys. J.* **2004**, *86*, 2530−2537.
(33) Han, D.; Pal, S.; Nangreave, J.; Deng, Z.; Liu, Y.; Yan, H. DNA Origami with Complex Curvatures in Three-Dimensional Space. *Science* **2011**, *332*, 342−346.
(34) Dietz, H.; Douglas, S. M.; Shih, W. M. Folding DNA into Twisted and Curved Nanoscale Shapes. *Science* **2009**, *325*, 725−730.
(35) Berger, R. M. L.; Weck, J. M.; Kempe, S. M.; Hill, O.; Liedl, T.; Rädler, J. O.; Monzel, C.; Heuer-Jungemann, A. Nanoscale FasL Organization on DNA Origami to Decipher Apoptosis Signal Activation in Cells. *Small* **2021**, *17*, 2101678.
(36) Wang, Y.; Baars, I.; Fördös, F.; Högberg, B. Clustering of Death Receptor for Apoptosis Using Nanoscale Patterns of Peptides. *ACS Nano* **2021**, *15*, 9614−9626.
(37) Kurisinkal, E. E.; Caroprese, V.; Koga, M. M.; Morzy, D.; Bastings, M. M. C. Selective Integrin $\alpha5\beta1$ Targeting through Spatially Constrained Multivalent DNA-Based Nanoparticles. *Molecules* **2022**, *27*, 4968.
(38) Schlichthaerle, T.; Lindner, C.; Jungmann, R. Super-Resolved Visualization of Single DNA-Based Tension Sensors in Cell Adhesion. *Nat. Commun.* **2021**, *12*, 2510.
(39) Kwon, P. S.; Ren, S.; Kwon, S.-J.; Kizer, M. E.; Kuo, L.; Xie, M.; Zhu, D.; Zhou, F.; Zhang, F.; Kim, D.; Fraser, K.; Kramer, L. D.; Seeman, N. C.; Dordick, J. S.; Linhardt, R. J.; Chao, J.; Wang, X. Designer DNA Architecture Offers Precise and Multivalent Spatial Pattern-Recognition for Viral Sensing and Inhibition. *Nat. Chem.* **2020**, *12*, 26−35.
(40) Comberlato, A.; Koga, M. M.; Nüssing, S.; Parish, I. A.; Bastings, M. M. C. Spatially Controlled Activation of Toll-like Receptor 9 with DNA-Based Nanomaterials. *Nano Lett.* **2022**, *22*, 2506−2513.
(41) Chaiet, L.; Wolf, F. J. The Properties of Streptavidin, a Biotinbinding Protein Produced by Streptomycetes. *Arch. Biochem. Biophys.* **1964**, *106*, 1−5.
(42) Bastings, M. M. C.; Helms, B. A.; van Baal, I.; Hackeng, T. M.; Merkx, M.; Meijer, E. W. From Phage Display to Dendrimer Display: Insights into Multivalent Binding. *J. Am. Chem. Soc.* **2011**, *133*, 6636−6641.
(43) Schmidt, T. G. M.; Koepke, J.; Frank, R.; Skerra, A. Molecular Interaction between the Strep-Tag Affinity Peptide and Its Cognate Target, Streptavidin. *J. Mol. Biol.* **1996**, *255*, 753−766.
(44) Voss, S.; Skerra, A. Mutagenesis of a Flexible Loop in Streptavidin Leads to Higher Affinity for the Strep-Tag II Peptide and Improved Performance in Recombinant Protein Purification. *Protein Eng. Des. Sel.* **1997**, *10*, 975−982.
(45) Eklund, A. S.; Comberlato, A.; Parish, I. A.; Jungmann, R.; Bastings, M. M. C. Quantification of Strand Accessibility in Biostable DNA Origami with Single-Staple Resolution. *ACS Nano* **2021**, *15*, 17668−17677.
(46) Vijaykumar, A.; ten Wolde, P. R.; Bolhuis, P. G. Generalised Expressions for the Association and Dissociation Rate Constants of Molecules with Multiple Binding Sites. *Mol. Phys.* **2018**, *116*, 3042−3054.
(47) Vanguri, V.; Govern, C. C.; Smith, R.; Huseby, E. S. Viral Antigen Density and Confinement Time Regulate the Reactivity Pattern of CD4 T-Cell Responses to Vaccinia Virus Infection. *Proc. Natl. Acad. Sci. U.S.A.* **2013**, *110*, 288−293.
(48) Jacobson, K.; Liu, P.; Lagerholm, B. C. The Lateral Organization and Mobility of Plasma Membrane Components. *Cell* **2019**, *177*, 806−819.
(49) Rice, A. M.; Mahling, R.; Fealey, M. E.; Rannikko, A.; Dunleavy, K.; Hendrickson, T.; Lohese, K. J.; Kruggel, S.; Heiling, H.; Harren, D.; Sutton, R. B.; Pastor, J.; Hinderliter, A. Randomly Organized Lipids and Marginally Stable Proteins: A Coupling of Weak Interactions to Optimize Membrane Signaling. *Biochim. Biophys. Acta, Biomembr.* **2014**, *1838*, 2331−2340.
(50) Alenghat, F. J.; Golan, D. E. Membrane Protein Dynamics and Functional Implications in Mammalian Cells. In *Current Topics in Membranes*; Elsevier, 2013; Vol. *72*, pp 89−120.
(51) Mackenzie, D. Proving the Perfection of the Honeycomb. *Science* **1999**, *285*, 1338−1339.
(52) Naskar, S.; Maiti, P. K. Mechanical Properties of DNA and DNA Nanostructures: Comparison of Atomistic, Martini and OxDNA Models. *J. Mater. Chem. B* **2021**, *9*, 5102−5113.
(53) Omori, S. A.; Cato, M. H.; Anzelon-Mills, A.; Puri, K. D.; Shapiro-Shelef, M.; Calame, K.; Rickert, R. C. Regulation of Class-Switch Recombination and Plasma Cell Differentiation by Phosphatidylinositol 3-Kinase Signaling. *Immunity* **2006**, *25*, 545−557.
(54) Xu, Z.; Zan, H.; Pone, E. J.; Mai, T.; Casali, P. Immunoglobulin Class-Switch DNA Recombination: Induction, Targeting and Beyond. *Nat. Rev. Immunol.* **2012**, *12*, 517−531.
(55) Yu, D.; Hung, M.-C. Overexpression of ErbB2 in Cancer and ErbB2-Targeting Strategies. *Oncogene* **2000**, *19*, 6115−6121.
(56) Ortega-Carrion, A.; Vicente-Manzanares, M. Concerning Immune Synapses: A Spatiotemporal Timeline. *F1000Research* **2016**, *5*, 418.
(57) Dustin, M. L.; Chakraborty, A. K.; Shaw, A. S. Understanding the Structure and Function of the Immunological Synapse. *Cold Spring Harbor Perspect. Biol.* **2010**, *2*, a002311.
(58) Owen, D. M.; Oddos, S.; Kumar, S.; Davis, D. M.; Neil, M. A. A.; French, P. M. W.; Dustin, M. L.; Magee, A. I.; Cebecauer, M. High Plasma Membrane Lipid Order Imaged at the Immunological Synapse Periphery in Live T Cells. *Mol. Membr. Biol.* **2010**, *27*, 178−189.

(59) Zhang, Z.; Liu, J.; Verlinde, C. L. M. J.; Hol, W. G. J.; Fan, E. Large Cyclic Peptides as Cores of Multivalent Ligands: Application to Inhibitors of Receptor Binding by Cholera Toxin. *J. Org. Chem.* **2004**, *69*, 7737−7740.

https://doi.org/10.1021/jacs.2c08529
J. Am. Chem. Soc. 2022, 144, 21576−21586